Mineralogy and petrology of shoshonitic lamprophyre dykes from the Sivarampeta area, diamondiferous Wajrakarur kimberlite field, Eastern Dharwar craton, southern India

Praveer PANKAJ*, Rohit Kumar GIRI*, N.V. CHALAPATHI RAO*, Ramananda CHAKRABARTI** and Sneha RAGHUVANSHI*

*Mantle Petrology Laboratory, Department of Geology, Centre of Advanced Study, Institute of Science, Banaras Hindu University, Varanasi-221005, India
**Centre for Earth Sciences, Indian Institute of Science, Bangalore-560012, India

Petrology and geochemistry (including Sr and Nd isotopes) of two lamprophyre dykes, intruding the Archaean granitic gneisses at Sivarampeta in the diamondiferous Wajrakarur kimberlite field (WKF), eastern Dharwar craton, southern India, are presented. The Sivarampeta lamprophyres display porphyritic-panidiomorphic texture comprising macrocrysts/phenocrysts of olivine, clinopyroxene (augite), and mica set in a groundmass dominated by feldspar and comprising minor amounts of ilmenite, chlorite, carbonates, epidote, and sulphides. Amphibole (actinolite-tremolite) is essentially secondary in nature and derived from the alteration of clinopyroxene. Mica is compositionally biotite and occurs as a scattered phase throughout. Mineralogy suggests that these lamprophyres belong to calc-alkaline variety whereas their bulk-rock geochemistry portrays mixed signals of both alkaline as well as calc-alkaline (shoshonitic) variety of lamprophyres and suggest their derivation from the recently identified Domain II (orogenic-anorogenic transitional type mantle source) from eastern Dharwar craton. Trace element ratios imply melt-derivation from an essentially the garnet bearing-enriched lithospheric mantle source region; this is further supported by their $^{87}Sr/^{86}Sr_{initial}$ (0.708213 and 0.708507) and 'enriched' $\varepsilon Nd_{initial}$ (−19.1 and −24.2) values. The calculated T_{DM} ages (2.7-2.9 Ga) implies that such enrichment occurred prior to or during Neoarchean, contrary to that of the co-spatial and co-eval kimberlites which originated from an isotopically depleted mantle source which was metasomatized during Mesoproterozoic. The close association of calc-alkaline shoshonitic lamprophyres, sampling distinct mantle sources, viz., Domain I (e.g., Udiripikonda) and Domain II (Sivarampeta), and kimberlites in the WKF provide further evidence for highly heterogeneous nature of the sub-continental lithospheric mantle beneath the eastern Dharwar craton.

Keywords: Mineralogy, Petrology, Lamprophyre, Dharwar craton, Southern India

INTRODUCTION

Lamprophyres constitute a diverse group of small volume, mantle-derived, volatile-rich, mafic-ultramafic, melanocratic, alkaline-igneous rocks, characterized by their porphyritic panidiomorphic texture consisting of hydrous mafic silicates (biotite and amphibole) with feldspar essentially confined to the groundmass (Rock, 1991; Woolley et al., 1996). A majority of the global lamprophyres are (i) spatially and temporally associated with other alkaline rocks such as nepheline-syenites, kimberlites, lamproites, and carbonatites, (ii) reported from diverse tectonic regimes, and (iii) play a key role in geodynamic interpretations (e.g., Garza et al., 2013; Stoppa et al., 2014; Krmicek et al., 2016; Pandey et al., 2019). Lamprophyres are often regarded to be products of partial melting of a metasomatized SCLM (sub-continental lithospheric mantle) to explain their high incompatible trace element content (Orejana et al., 2008; Owen, 2008; Li et al., 2014; Ma et al., 2014; Muller and Groves, 2019), and therefore their geochemistry play a significant role in understanding the evolution of SCLM. Alkaline, calc-alkaline, and ultramafic varieties constitute the three lamprophyre clans whereas shoshonitic lamprophyres-which are considered as variants of calc-alkaline lamp-

doi:10.2465/jmps.191004b
N.V. Chalapathi Rao, nvcrao@bhu.ac.in Corresponding author

rophyres-often display mixed affinity to both alkaline and calc-alkaline lamprophyres (see Rock, 1987, 1991; Pandey et al., 2017b).

The eastern Dharwar craton (EDC) of southern India is one of the extensively well-studied Precambrian granite-greenstone terrains of the Indian shield. Lamprophyres in the EDC are mainly confined to two regions (Fig. 1a); (i) the Prakasam alkaline Province or the Cuddapah intrusive province towards the eastern margin of the Paleo-Mesoproterozoic Cuddapah basin at the junction of the EDC with Eastern Ghat granulite (mobile) belt where the lamprophyres are essentially of alkaline variety with a few of them displaying shoshonitic character (Madhavan et al., 1998; Chalapathi Rao, 2008) and (ii) towards the western margin of the Cuddapah basin within the diamondiferous Wajarakarur kimberlite field where the lamprophyres of calc-alkaline and/or shoshonitic nature are reported (Pandey et al., 2017a, 2017b, 2018a and references therein).

Lamprophyres towards the western margin of the Cuddapah basin are relatively less studied compared to those from the Prakasam Alkaline Province at the eastern margin. Recent studies (Pandey et al., 2017a, 2017b, 2018a, 2018b; Raghuvanshi et al. 2019) on lamprophyres from the western margin of the Cuddapah basin have brought out involvement of three distinct mantle source domains in their genesis; (a) Domain I: represented by orogenic calc-alkaline and/or shoshonitic lamprophyres (e.g., Mudigubba, Udiripikonda, and Kadiri) derived from the SCLM, (b) Domain II: represented by orogenic-anorogenic, alkaline to calc-alkaline lamprophyres (e.g., Korakkodu) sampling mixed orogenic-anorogenic transitional source, and (iii) Domain III: represented by alkaline lamprophyres (e.g., Ankiraopalli) displaying a strong OIB type (asthenospheric) overprint on the SCLM source (see Giri et al. 2019). The present study on the Sivarampeta lamprophyre dykes, located within diamondiferous Mesoproterozoic-Late Cretaceous Wajrakarur kimberlite field (WKF), assumes importance in this context. In this paper, mineral chemistry, bulk-rock, and radiogenic isotopic (Sr-Nd) geochemistry of the Sivarampeta lamprophyre (SPL) dykes are presented. Our aim is to explore the petrogenetic relationship, if any, between the hitherto studied lamprophyres and the co-spatial kimberlites of the WKF and compliments similar recent studies carried on calc-alkaline and/or shoshonitic lamprophyres at the Mudigubba, the Kadiri, the Korakkodu, and the Udiripikonda areas towards the western margin of the Cuddapah basin in the EDC (Pandey et al., 2017a, 2017b, 2018a, 2018b; Khan et al., 2018; Raghuvanshi et al., 2019). We also attempt to understand the nature of mantle source of the Sivarampeta lamprophyres vis-à-vis recently identified three distinct lamprophyre source domains from the EDC (see Giri et al. 2019).

GEOLOGICAL BACKGROUND

The Dharwar Craton of southern India (Fig. 1) preserves a huge oblique section of pristine Archean crust spanning from 3.8-2.5 Ga which transitions from the lower to upper crustal levels and comprises Meso-Neoarchean greenstone belts intruded by younger granitoids (Swami Nath et al., 1976; Jayananda et al., 2018 and references therein; Peng et al. 2019). Main lithological associations reported here are TTGs and transitional TTGs, bimodal volcanic-sedimentary greenstone sequences, and composite plutons of sanukitiods and anatectic granites (Ramakrishnan and Vaidyanadhan, 2008; Jayananda et al., 2013, 2018 and references therein). Even though the Dharwar craton for long was divided into two or even three blocks- the eastern and the western Dharwar, recent studies (see Peucat et al., 2013; Ishwar Kumar et al., 2013; Santosh et al., 2015; Roberts and Santosh, 2018; Jayananda et al., 2018 and references therein) favour it to be an amalgamation of several micro-blocks (western, central, eastern, Coorg and Karwar) with independent thermal record and evolutionary histories. Peng et al. (2019) envisaged the Dharwar craton to be a trinity of Archean crustal architecture ('sandwich' structure), comprising (i) 2700-2500 Ma-dominated upper crust, (ii) 3400-2900 Ma-dominated middle crust, and (iii) ~ 2560-2500 Ma anatectic lower crust. Peng et al. (2019) further proposed that this 'sandwich' structure possibly indicates vertical growth of the crust in the Archean.

The eastern block is comparatively thinner and relatively younger than western and central blocks and comprises a collage of greenstone belts with lesser volcanics, Paleo-Mesoproterozoic Purana sedimentary basins, and various mafic dyke swarms of different Paleoproterozoic magmatic episodes together with Mesoproterozoic intrusions of kimberlites, lamproites, and lamprophyres. Available geochronological data suggest that the age of these kimberlites, lamproites, and lamprophyres span from 1.38 to 1.1 Ga (Osborne et al., 2011; Chalapathi Rao et al., 2013 and references therein). However, a Late Cretaceous kimberlite event linked to Marion hotspot activity at ~ 90 Ma has also been recently recorded from the WKF (Chalapathi Rao et al., 2016).

This paper focuses on mineral chemistry, geochemistry, and isotope (Sr-Nd) geochemistry of two lamprophyre dykes-termed henceforth as SPL (Fig. 1b; Toposheet no. 57 F/5;14°50′43.8″N; 77°19′50.7″E and 14°50′43.7″N; 77°19′57.8″E) exposed in the Sivarampeta area, within and in the vicinity of WKF, SPL intrude

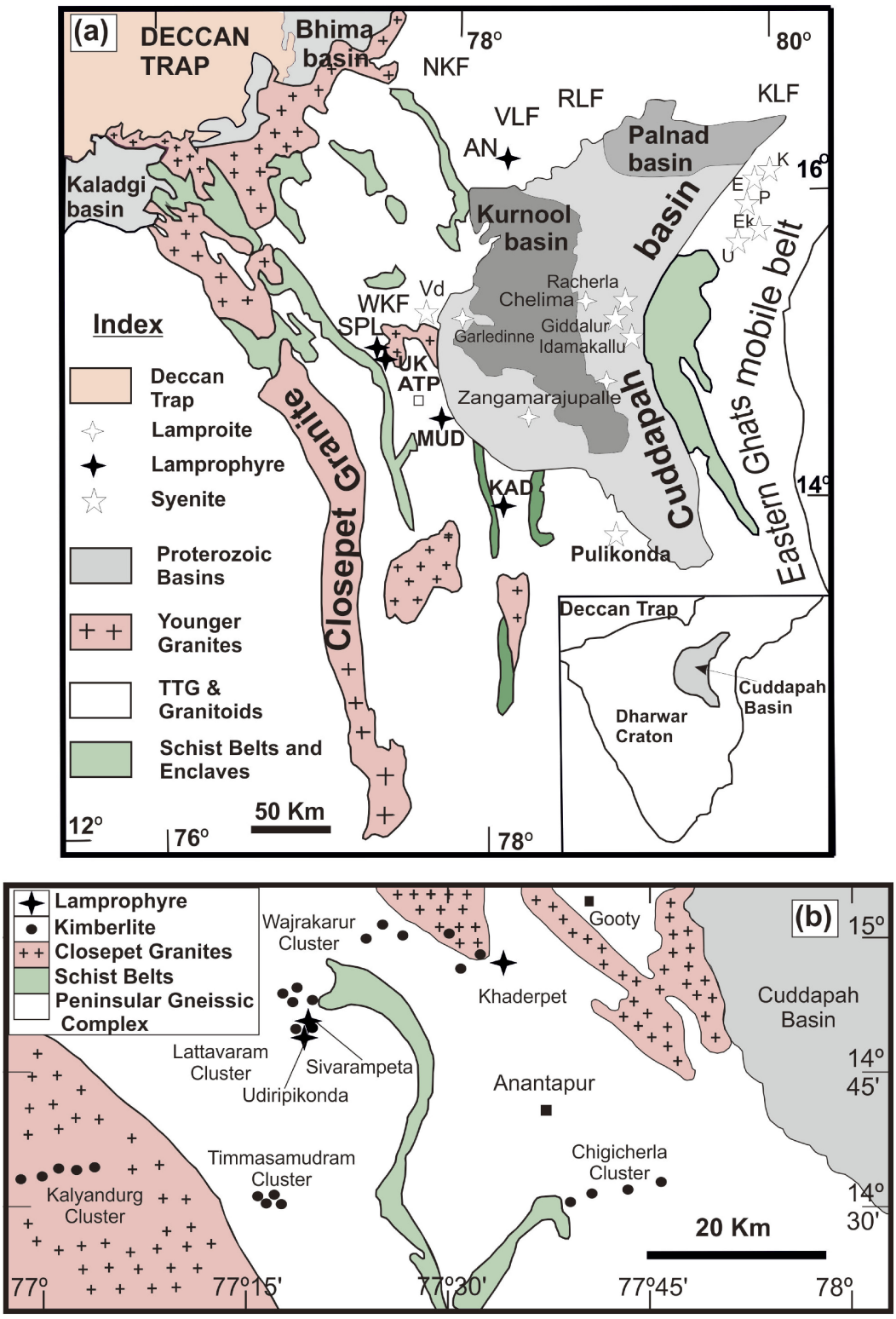

Figure 1. (a) Generalized geological map of peninsular India (modified after Naqvi, 2005) showing Eastern Dharwar craton (EDC), Palaeo–Mesoproterozoic Cuddapah basin and disposition of various alkaline–subalkaline, mafic–ultramafic rocks and location of Sivarampeta lamprophyres (SPL). NKF, Narayanpet kimberlite field; VLF, Vattikode lamproite field; RLF, Ramadugu lamproite field; KLF, Krishna lamproite field; MUD, Mudigubba lamprophyre; AN, Ankiraopalli lamprophyre; RKF, Raichur kimberlite field; UK, Udiripikonda lamprophyre; WKF, Wajrakarur kimberlite field. (b) Geological map (after Nayak and Kudari, 1999) showing Sivarampeta lamprophyre confined to the Lattavaram cluster of Wajrakarur kimberlite field. Location of Ankiraopalli and Khaderpet lamprophyre are taken from Giri et al. (2019) and Khan et al. (2018) respectively. Other fields are taken from Pandey et al. (2017b).

the granite gneisses of the basement Peninsular Gneissic Complex (Figs. 2a and 2b) and are melanocratic with shining pyroxene crystals.

ANALYTICAL TECHNIQUES

We have collected fresh rock samples from the Sivarampeta lamprophyre dykes. Various mineral phases present in the SPL polished thin sections were studied out by optical microscope prior to electron microprobe (EPMA) analysis. Minerals were analyzed at Mantle Petrology Laboratory, Department of Geology, Banaras Hindu University, Varanasi, using a CAMECA-SXFive wavelength-dispersive electron microprobe (EPMA) with several crystals and LaB6 filament source (see Appendix 1 in Giri et al., 2019, for analytical details). Based on multiple analysis the error has been reduced <1% on major element concentrations, whereas for trace element the error ranges between 3 and 5%. The representative mineral composition is presented in Supplementary Table S1 (available online from https://doi.org/10.2465/jmps.191004b).

For bulk-rock geochemistry, four fresh rock samples-two from each dyke, were powdered at the Department of Geology, Banaras Hindu University, using Retsch BB50 jaw crusher and Retsch RM100 motor grinder and analyzed at the Activation Laboratories, Ancaster, Canada. Alkaline fusion and ICP-OES analysis (Model: Thermo-Jarrell-Ash ENVIRO II) and multi-acid digestion and ICP-MS analysis (Model: Perkin Elmer Sciex ELAN 6000) were used for measurement of major, trace, and rare-earth element concentrations, respectively. STM1 MRG1, DNC1, W2, and SY3 were the external standards used to monitor the accuracy and precision, which was ~ 5% for major oxide and 5-10% for trace elements. Bulk-rock major and trace element data are presented in Table S1.

Isotopic analyses (Sr-Nd) of two of the representative samples were performed at the Center for Earth Sciences, Indian Institute of Science, Bangalore, following the same protocol as described in Banerjee et al. (2016) using an Inductively Coupled Plasma Mass Spectrometer (ICP-MS). Accuracy and precision for both major and trace element are illustrated with the repeated analysis of samples and standards, and instrumental mass fractionation were rectified by normalizing the measured value. During the course of the analysis, JNdi-1 Nd isotopic-standard analyzed yielded $^{143}Nd/^{144}Nd = 0.512120 \pm 7$ (2SD, n = 3) while SRM-987 Sr isotopic-standard analyzed yielded $^{87}Sr/^{86}Sr = 0.710260 \pm 9$ (2SD, n = 3) value. $^{86}Sr/^{88}Sr = 0.1194$ were used as normalizing parameters to normalize measured $^{87}Sr/^{86}Sr$ ratio, and $^{146}Nd/^{144}Nd = 0.7219$ were used for $^{143}Nd/^{144}Nd$ ratios respectively. The results obtained are provided in Table S1.

RESULTS

Petrography and mineral chemistry

Petrography of the SPL reveals porphyritic and panidiomorphic texture typical of lamprophyres with pyroxenes as the dominant mafic phenocrysts, followed by macrocrysts of olivine, and feldspar confined to the groundmass (Figs. 2c and 2d). Mica, ilmenite and secondary amphibole occur as scattered phases in the groundmass along with carbonate and chlorite. A majority of the olivines are replaced by carbonate and often rimmed with serpentine (Fig. 2d). Pyroxenes are mostly zoned, and some of them display twinning (Figs. 2e and 2f) and at places also form clusters giving rise to glomeroporphyritic texture (Fig. 2c). Amphibole occurs as an alteration product of pyroxene and belongs to actinolite-tremolite association (Fig. 2g). Mica and ilmenite are scattered in the groundmass (Fig. 2h). Each of these phases and their composition are individually discussed below.

Olivine. Petrographic studies reveal that olivine occurs as macrocyst as well as phenocryst. All of the phenocrystic olivine are pseudomorphed and thus unsuitable for mineral chemistry studies. However, we could locate a single preserved pristine macrocrystic olivine grain very likely derived from mantle peridotite (Fig. 2d), and the absence of compositional zoning further attests their derivation from mantle peridotite. Microprobe study reveals it to be mainly forsteritic with a restricted compositional range (see Supplementary Table S1) In the Fo content versus NiO (wt%) plot (Fig. 3a), it is confined to mantle olivine array (Takahashi et al., 1987) and is clearly distinct from those of metamorphic olivine array (Pelletier et al., 2008). Olivine of the SPL, however, has a lower Fo content when compared to those from peridotite xenoliths reported from kimberlites of WKF (Ganguly and Bhattacharya, 1987). Color-coded X-ray elemental images (Supplementary Fig. S1; available online from https://doi.org/10.2465/jmps.191004b) show enrichment of silica, depletion of iron, magnesium in its rim, and bringing out serpentinization.

Pyroxenes. Pyroxene occurs as a dominant mafic pristine euhedral phenocrystic phase. Mineral chemistry of the pyroxenes reveal their restricted variation and uniform composition ($Wo_{40.28-41.67}En_{45.55-49.25}Fs_{7.37-9.90}Ac_{2.22-3.06}$) (see Table S1). In the ternary pyroxene discrimination diagram (after Morimoto, 1988) (see Fig. 3b) most of the pyroxenes fall in the field of augite and rarely in the field of diopside. Clinopyroxenes of SPL are also clearly indistinguishable from those of other Dharwar and Deccan lamprophyres (Fig. 3b). SPL clinopyroxene also shows overlap with those from global ultramafic and calc-alkaline lamp-

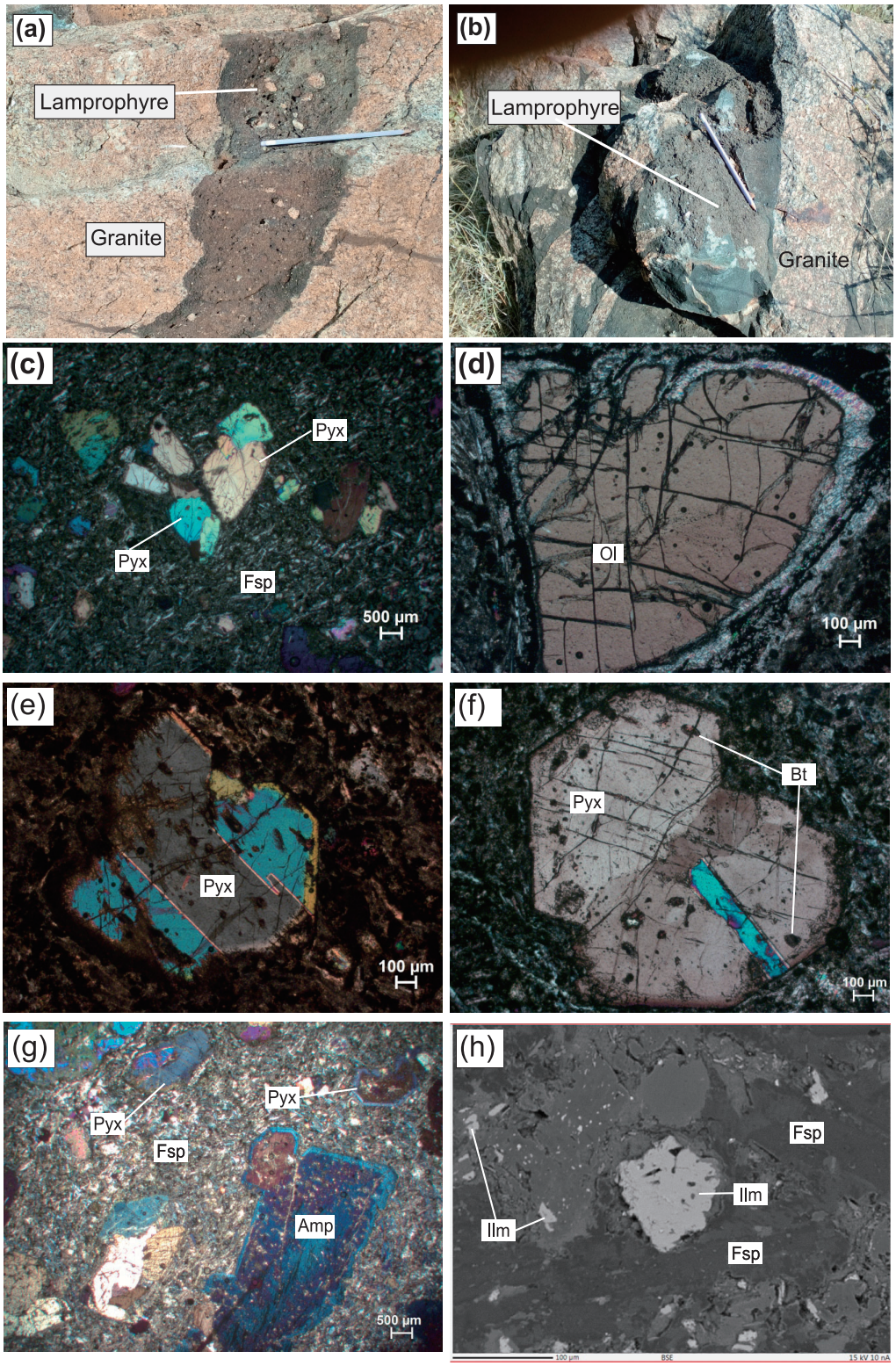

Figure 2. Field photographs of Sivarampeta lamprophyres (SPL). (a) Lamprophyre dyke intruding into the granite. (b) Close view showing patches of SPL in the granite. Photomicrographs of SPL depicting various textural and mineralogical aspects. (c) Glomeroporphyritic cluster of pyroxenes in a plagioclase-dominating groundmass (crossed polars). (d) Photomicrograph showing a bigger olivine grain with serpentinized rim (crossed polars). (e) Pyroxene showing twinning (crossed polars) in a feldspar-rich groundmass. (f) Phenocryst of pyroxene showing zoning and inclusions of biotite (crossed polars) (g) Secondary amphiboles with relict texture (crossed polars). (h) Back scattered electron (BSE) image showing pristine and euhedral ilmenite. Ol, Olivine; Pyx, Pyroxene; Bt, Biotite; Amp, Amphibole; Fsp, Feldspar; Cal, calcite; Ilm, Ilmenite.

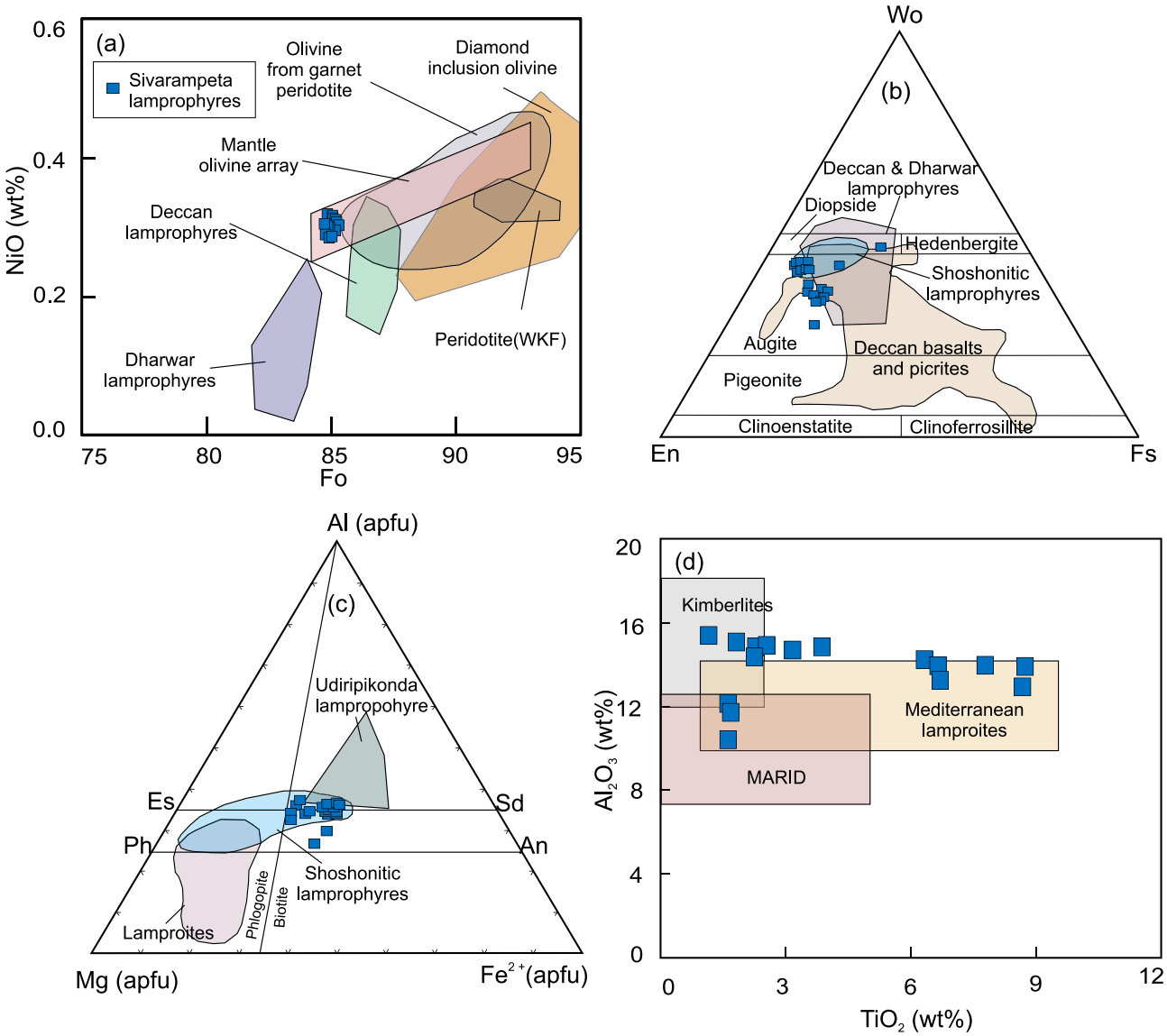

Figure 3. (a) Fo (mol%) versus NiO (wt%) content of olivine macrocrysts. The field of mantle olivine array is after Takahashi et al. (1987); Field of Deccan UML after Pandey et al. (2018b); Field of Diamond inclusion olivines and those from garnet peridotite are taken from Rudnick et al. (1994); Field for Garnet peridotite xenoliths from 1100 Ma Kimberlites from the WKF, eastern Dharwar craton are taken from Ganguly and Bhattacharya (1987), Data for Dharwar lamprophyres is after Pandey et al. (2017b). (b) Conventional compositional discriminatory ternary diagram for clinopyroxene in terms of molar Wo-En-Fo (after Morimoto, 1988) for SPL, comparing them with worldwide shoshonitic lamprophyre (Rock, 1991), clinopyroxenes of Dharwar lamprophyres (Pandey et al., 2017a, 2017b), Deccan lamprophyres (Pandey et al., 2019 and references therein) and fields of Deccan basalts and picrites are from Dongre et al. (2017). (c) Mica compositional discrimination ternary diagram in terms of Al-Mg-Fe^{2+} showing it to be dominantly of biotite type and Mg-rich nature compared to that of Udiripikonda shoshonitic lamprophyres (after Pandey et al., 2017b) and compositional ranges for mica of shoshonitic lamprophyres and lamproites worldwide (from Rock, 1991). (d) Mg# versus Al_2O_3 (wt%) discrimination diagram (after Rock, 1986) with various fields is from Rock (1987, 1991). Es, eastonite; Ph, phlogopite; Sd, siderophyllite; An, annite.

rophyres (Supplementary Fig. S2a; available online from https://doi.org/10.2465/jmps.191004b). On the other hand, the Ca versus Ti (apfu) (Fig. S2b) discriminatory diagram (after Sun and Bertrad, 1991) suggests an orogenic origin for these clinopyroxenes. Color-coded X-ray elemental images (Figs. S2c-S2h) of clinopyroxene grains show an absence of sodium, depletion of aluminum, and magnesium, followed by enrichment of iron and titanium in the rim when compared to those in the core.

Mica. Mica is present as in the groundmass as well as inclusions in pyroxene. Mica show variation in its TiO_2 (8.72-1.63 wt%), FeO (19.00-12.82 wt%), and Al_2O_3 (15.10-10.49 wt%) as well as in its Mg# (48-63) (see Table S1). In the Al-Mg-Fe^{2+} mica classification di-

agram (Fig. 3c), the SPL mica is (i) confined to the field of biotite, (ii) indistinguishable from those of world-wide shoshonitic lamprophyres, (iii) comparable to that of the Udiripikonda lamprophyre, and (iv) clearly distinct from those of world-wide lamproites (Rock, 1991). The SPL mica show compositional similarity with that of kimberlites (Mitchell, 1995), Mediterranean lamproites, and MARID (mica-amphibole-rutile-ilmenite-diopside) suite of rocks (Dawson and Smith, 1977) and has less TiO_2 content than that of the Udiripikonda lamprophyre (Fig. 3d). The SPL mica overlays compositional fields of those from alkaline as well as calc-alkaline lamprophyres but is distinguishable from that of ultramafic lamprophyres and lamproites (Supplementary Fig. S3a; available online from https://doi.org/10.2465/jmps.191004b).

Amphibole. Amphiboles are subhedral and essentially secondary in nature (actinolite-tremolite). Petrography reveals relict texture and suggests that these amphiboles are alteration products of the primary pyroxene (Fig. 2g). In the SiO_2 wt% versus TiO_2 wt% discriminatory diagram (Table S1 and Fig. S3b, after Leake et al., 1997), they show compositional overlap with the secondary amphiboles, whereas, in the Si (apfu) versus Mg# (after Leake et al., 1997; Fig. S3c) classification plot, they are confined to the fields of actinolite.

Feldspar. Representative mineral chemistry data suggest feldspars be dominantly Na-rich and Ca-poor plagioclases (see Table S1). The composition of feldspar analyzed range from albite to anorthoclase type ($Or_{0.11-94.31}$ $Ab_{5.69-98.23}An_{0.00-5.91}$) with a minor amount of sanidine (Fig. S3d).

Ilmenite. Ilmenite is scattered in the groundmass. It has a restricted range of TiO_2 (51.81-50.28 wt%), FeO (48.12-42.84 wt%) and very low content MnO (1.33-3.42 wt%), and Cr_2O_3 (0.14-0.20 wt%) (see Table S1). Its Ti-Fe rich nature confines it to be ilmenite sensu stricto in the ternary classification diagram (Fe_2O_3-FeO-TiO_2) (Fig. S3e).

Other mineral phases. Other mineral phases present in minor amount include serpentinite, chlorite, carbonate, epidote, and sulphides.

Bulk-rock geochemistry

The bulk-rock (major and trace) data of the representative samples of the SPL are provided in Table S1. The SPL have a restricted and low range of SiO_2 content varying between 47.21-47.97 wt%. The SPL samples have high K_2O (2.89-3.43 wt%), Na_2O (2.92-3.48 wt%) and CaO (7.65-9.02 wt%) contents. Owing to their high K_2O content, in the K_2O versus SiO_2 classification diagram (Fig. 6a, after Peccerillo and Taylor, 1976), they are confined

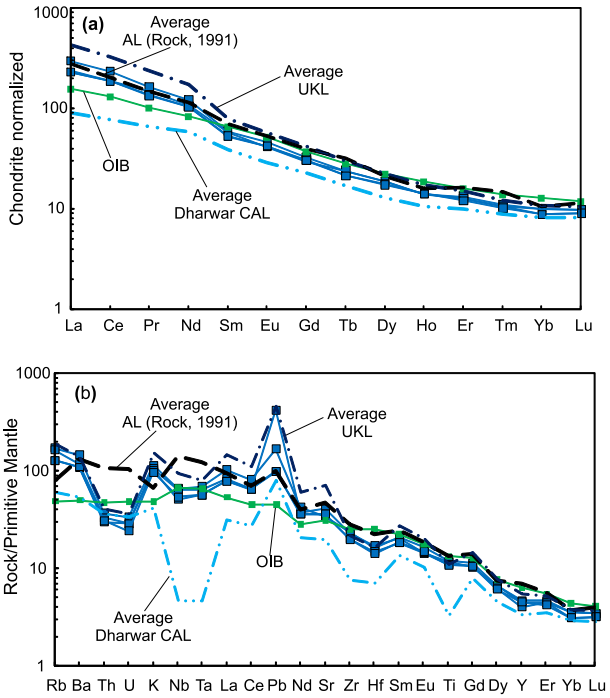

Figure 4. (a) Chondrite-normalized REE patterns. Normalization values are from Sun and McDonough (1989). (b) Primitive mantle-normalized trace element diagrams for the SPL Normalization values are from Sun and McDonough (1989). Other data sources are the same as in Figure 3.

to the shoshonitic field and resemble co-spatial Udiripikonda shoshonitic lamprophyres (Pandey et al., 2017b). When compared to the global calc-alkaline, ultramafic, alkaline lamprophyres, and the Superior Province Archaean calc-alkaline lamprophyres, the SPL samples, however, display mixed signals (Fig. 6b) without confining to any particular field. A limited variation in MgO (6.14-8.20 wt%) content along with moderate Mg# (54.09-61.42) and high Cr (>150 ppm) and Ni (>170 ppm) coupled with high LILE, high Ba (758-1024), and Sr (723-854) typically suggest their origin from an enriched magma source (Table S1, Figs. 4a and 4b).

Sr-Nd isotope geochemistry

Measured Nd and Sr isotopic data of the two representative SPL samples are provided in Table S1. We have calculated the initial Nd and Sr isotope ratios by assuming an emplacement age of 1100 Ma based on location of the SPL in close vicinity to the ~ 1100 Ma kimberlite from the WKF and by assuming that they belong to the same tectono-magmatic episode. Age-corrected $^{143}Nd/^{144}Nd$ values are 0.510244 and 0.509978, and $^{87}Sr/^{86}Sr$ values are 0.708213 and 0.708507. However, strongly negative ϵ_{Nd} values of −19.1 and −24.2 indicate effects of either

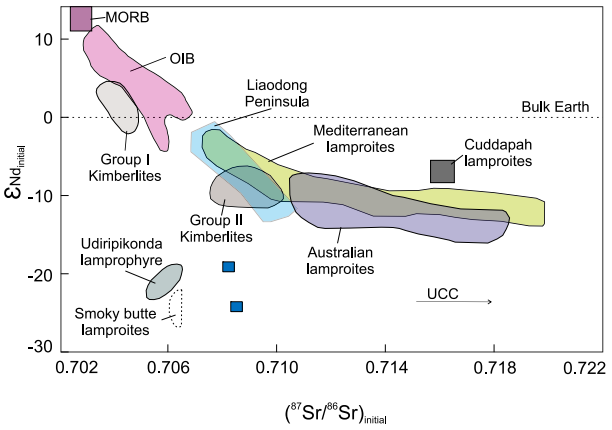

Figure 5. Initial $^{87}Sr/^{86}Sr_{initial}$ versus $\varepsilon Nd_{initial}$ isotope variation diagram for SPL. Fields are same as given in Figure 9. Other data sources are taken from Cuddapah lamproites (Chalapathi Rao et al., 2004); other fields are from Gibson et al. (1995), Gibson et al. (2006), and Pandey et al. (2017b) and references therein.

source contamination and/or crustal assimilation during the magma ascent.

DISCUSSION

Crustal contamination and post-magmatic alteration

Crustal contamination and alteration (dueteric) of minerals in lamprophyres during emplacement is a common process (Rock, 1991; Moyen et al., 2003). Therefore, it is necessary to assess the effect of crustal contamination and alteration before the interpretation of geochemical data. Petrographical aspects such as serpentinization of olivine, and replacement of clinopyroxenes by amphiboles suggest post-magmatic alteration (Fig. 2). As petrography exclude crustal xenoliths, we prefer mantle source contamination by subducted material to be the likely causative factor. The calculated T_{DM} ages range from 2754 to 2984 Ma and imply that the source enrichment occurred during Neoarchean (2800–2600 Ma) (Fig. 5). Crustal rocks are known to be enriched in LILEs, have negative Nb and Ta anomalies, whereas their major oxides show high content of K_2O and Na_2O with a depleted TiO_2 and P_2O_5 contents. However, a high concentration of REE and incompatible trace elements, and lower degrees of partial melting, make lamprophyres insensitive to crustal contamination. Primitive mantle normalized multi-element plot (Fig. 4a) lack negative Nb and Ta anomalies and excludes significant crustal contamination of the SPL samples. This is further supported by the restricted ranges of SiO_2 (47.21–47.97 wt%), MgO (6.14–8.20 wt%), TiO_2 (2.31–2.55 wt%), and P_2O_5 (0.48–0.58 wt%) contents which clearly contrast with those of continental crust. Higher Nb/U (60.00–76.67) and Ce/Pb (3.80–16.57) of SPL samples also are different from those of crustal values (Nb/U = 6.15; Ce/Pb = 3.91, Rudnick and Gao, 2003). The Nb versus Nb/U and Ce versus Ce/Pb diagrams (Figs. 6c and 6d) demonstrate the similarity of SPL samples with those of the OIB suggesting insignificant crustal contamination. Figures 6c and 6d also shows that the SPL samples are comparable with those of the Udiripikonda lamprophyres rather than the Mudigubba or the Chotaudepur (Deccan) lamprophyres in their trace element content.

Classification and Tectonic significance

Petrography reveals that studied SPL samples belong to the calc-alkaline variety of lamprophyres in general and kersantite in particular (Rock, 1991; Le Maitre, 2002). Mineral chemistry of mafic phases like clinopyroxene and mica, and bulk rock geochemistry suggests an overprinting of both calc-alkaline and alkaline signatures (Figs. 6a and 6b). In fact, mineral chemistry of clinopyroxene and micas are indistinguishable with those of global shoshonitic lamprophyres and the Udiripikonda lamprophyre suggesting the SPL samples to display a shoshonitic character.

Lamprophyres are found in all possible tectonic regimes and their geochemistry is widely used to discriminate between orogenic vs anorogenic tectonic settings (Muller and Groves, 2019 and references therein). Tectonic discrimination diagrams involving TiO_2/Al_2O_3 versus Zr/Al_2O_3 and Hf-Th-Nb/2 (see Fig. 8b and Supplementary Fig. S4; available online from https://doi.org/10.2465/jmps.191004b) clearly reveal that SPL samples (i) have high Ti and Nb content in comparison to those of Dharwar calc-alkaline lamprophyres (Mudigubba and Kadiri), (ii) are indistinguishable from those of the Udiripikonda shoshonitic lamprophyre and are comparable to the Deccan lamprophyres, and (iii) have an anorogenic intra-plate type of tectonic setting.

Mantle source and petrogenesis

Moderate to higher Mg# (54–61) and higher Nb/U (60.00–76.67), Ce/Pb (3.80–16.57), Al_2O_3/TiO_2 (5.6–5.9) of the SPL samples contrast with those of crustal values (Nb/U = 6.15; Ce/Pb = 3.91; Al_2O_3/TiO_2 = 24.1, Zr/Nb = 16.08 and Th/La = 0.28; Rudnick and Gao, 2003) and suggest their derivation from a mantle source. The abundance of incompatible elements and high REE fractionation (Fig. 4a) and strongly negative ϵ_{Nd} values of −19.1 and −24.2 (Fig. 5) imply the involvement of an enriched mantle source. High TiO_2 (2.31–2.55 wt%), Nb (36–47 ppm),

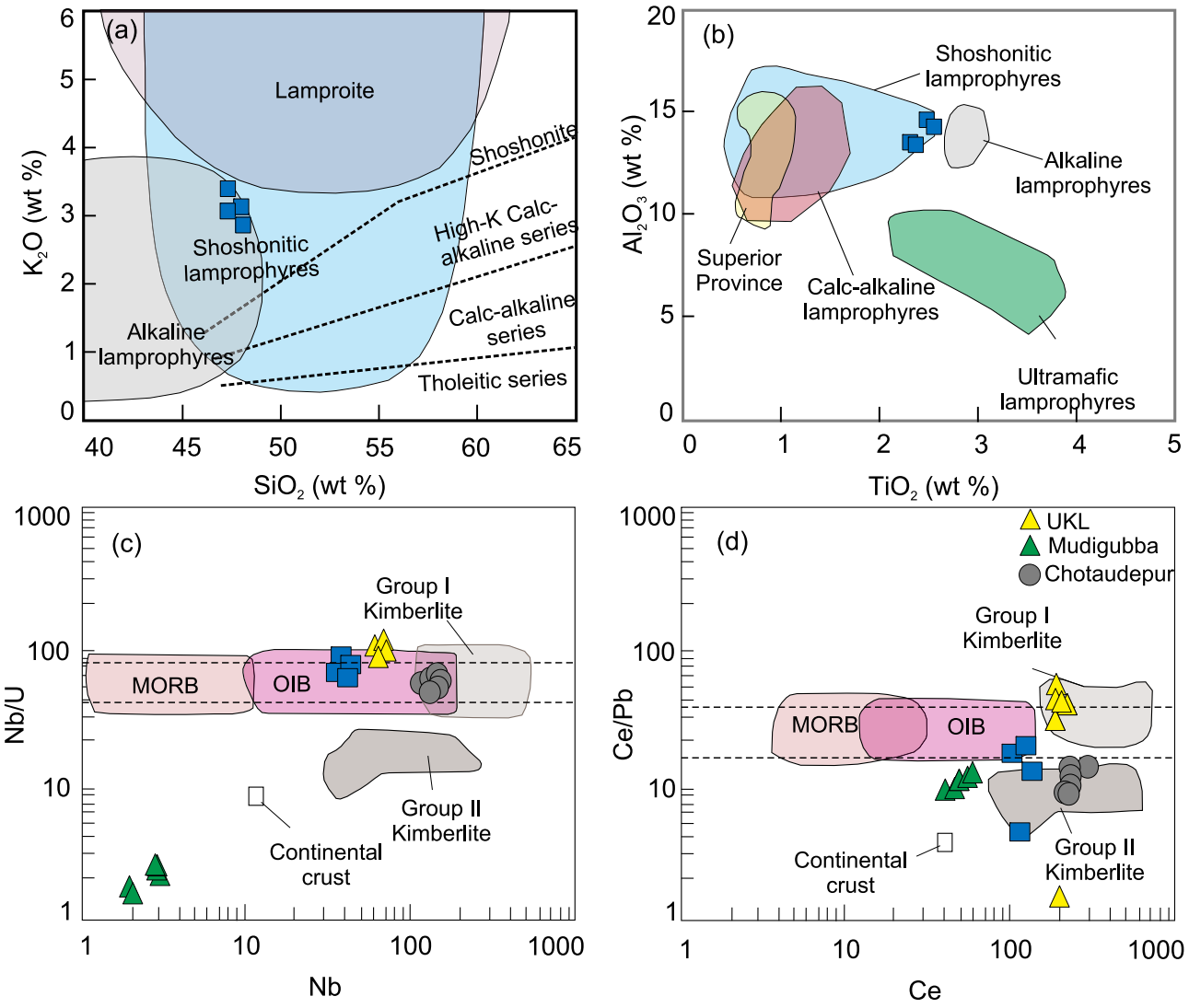

Figure 6. (a) K_2O (wt%) versus SiO_2 (wt%) diagram (Peccerillo and Taylor, 1976) showing shoshonitic character of SPL, classification scheme is based on Rock (1987). (b) TiO_2 (wt%) versus Al_2O_3 (wt%) diagram (after Rock, 1987) classifying AN as alkaline lamprophyres (ALs), while other fields are shown for comparison. Data sources: CAL, Calc-alkaline lamprophyres; AL, Alkaline lamprophyres; UML, Ultramafic lamprophyres. Archaean CAL from different cratons are taken from Lefebvre et al. (2005) and references therein. Data for shoshonitic lamprophyres are taken from Rock (1991), Wyman and Kerrich (1993), Jiang et al. (2010), and Taylor et al. (1994). Data Sources for Superior province is from Wyman and Kerrich (1989). (c) Nb (ppm) versus Nb/U and (d) Ce (ppm) versus Ce/Pb diagram (after Su et al., 2017) for the SPL showing uncontaminated nature. Various fields are taken from Le Roex et al. (2003). Data sources for Udiripikonda lamprophyre (UKL) (after Pandey et al., 2017b), Mudigubba lamprophyre (MUD) (after Pandey et al., 2017a) and Chotaudepur lamprophyre (after Chalapathi Rao et al., 2012).

La (54–70.2 ppm), with higher La/Yb (33.24–41.29) and lower Nb/La (0.67–0.81) suggest the involvement of asthenospheric-mantle. The bi-variate source discrimination plot (Figs. 7a and 7b) involving La/Yb versus Nb/La (Karsli et al., 2014) suggests mantle source of a mixed sub-continental lithosphere and asthenosphere. Figures 7a and 7b also reveal contrasting character of SPL with those of (i) the calc-alkaline lamprophyres present in the eastern Dharwar craton (which have relatively low content of Nb/La) and (ii) the Deccan lamprophyres (which have higher Nb/La). However, this mixed lithopheric-asthenospheric contribution in the mantle source region of the SPL imply a close affinity to the nearby Udiripikonda shoshonitic lamprophyre and the Superior Province shoshonitic lamprophyres.

Ba/Rb and Rb/Sr of SPL suggest the presence of mica in the mantle source (Fig. 7b). Primitive mantle-normalized trace element average ratios $(Hf/Sm)_{PM}$ (0.80) and $(Ta/La)_{PM}$ (0.72) of the SPL samples are slightly enriched than those of the mantle values (Hf/Sm = 0.80;

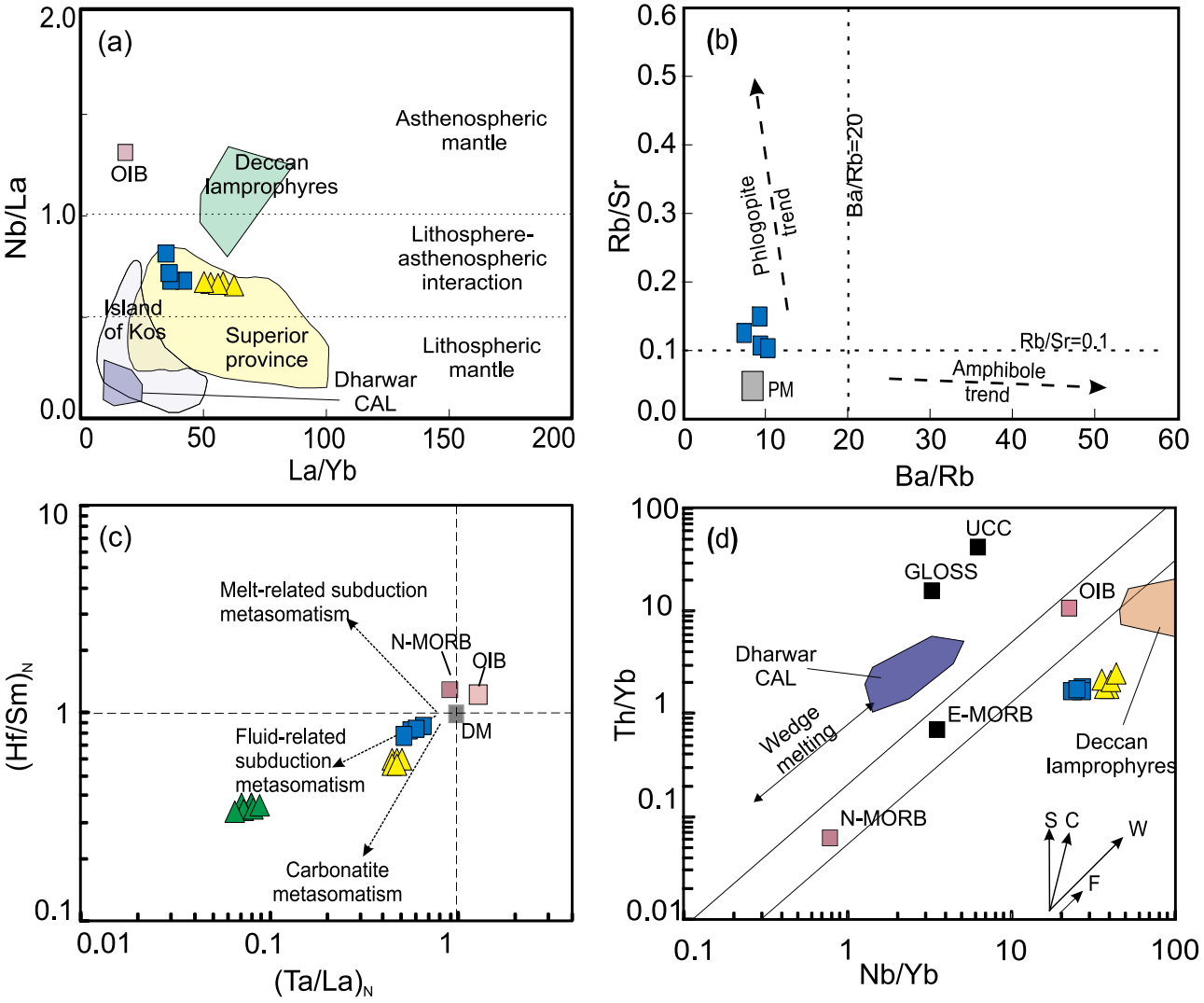

Figure 7. (a) La/Yb versus Nb/La plot (after Karsli et al., 2014) ruling out significant asthenospheric contribution in the mantle source region of the SPL and showing its close affinity to the Udiripikonda lamprophyres. (b) Ba/Rb versus Rb/Sr plot (Ma et al., 2014) showing the presence of mica in the mantle source of the SPL. (c) $(Ta/La)_{PM}$ versus $(Hf/Sm)_{PM}$ diagram (after La Flèche et al., 1998), (d) Nb/Yb versus Th/Yb diagram (after Pearce, 2008). Data sources are the same as in Figure 6.

Ta/La = 0.06, Sun and McDonough, 1989) suggesting an incompatible trace element enriched source. In the $(Ta/La)_{PM}$ versus $(Hf/Sm)_{PM}$ bivariate plot (Fig. 7c) discriminating, different types of metasomatism (melt-related subduction, fluid-related subduction, and carbonatitit-ic), effects of fluid-related subduction metasomatism are brought out. Figure 7c also reveal a closer association of the SPL trace element ratios with those of the Udiripikonda shoshonitic lamprophyre than those from the Kadiri and the Mudigubba calc-alkaline lamprophyres. However, in the Nb/Yb versus Th/Yb bi-variate diagram (see Fig. 7d, after Pearce, 2008), the SPL samples (i) are closer to the mantle array, (ii) display with-in-plate association, (iii) overlap with the field of the Udiripikonda lamprophyre, and (iv) contrast with the other Dharwar calc-alkaline lamprophyres, UCC (upper continental crust) and GLOSS (global oceanic subducting sediment).

Low Al_2O_3/TiO_2 (5.6-5.9), Sc (14-19 ppm), Y (18-21 ppm), and Lu/Hf (0.048-0.053) along with moderately high primitive mantle normalized ratios $(Gd/Yb)_N$ (2.96-3.47) and fractionated heavy-REE $(Dy/Yb)_N$ (1.89-2.01), $(Sm/Y)_N$ (4.15-4.56) suggest an enriched mantle source with a garnet signature and high La/Yb (36-41) ratio implies lower degrees of partial melting (McKenzie and O'Nions 1991). We have calculated the extent of partial melting assuming non-modal batch melting of a garnet-bearing PM (Primitive mantle) (Sun and McDonough, 1989) and EAM (enriched asthenospheric mantle) (Seghedi et al., 2004) (Fig. 8a) as source compositions (see Miller et al., 1999). The calculated trace element model

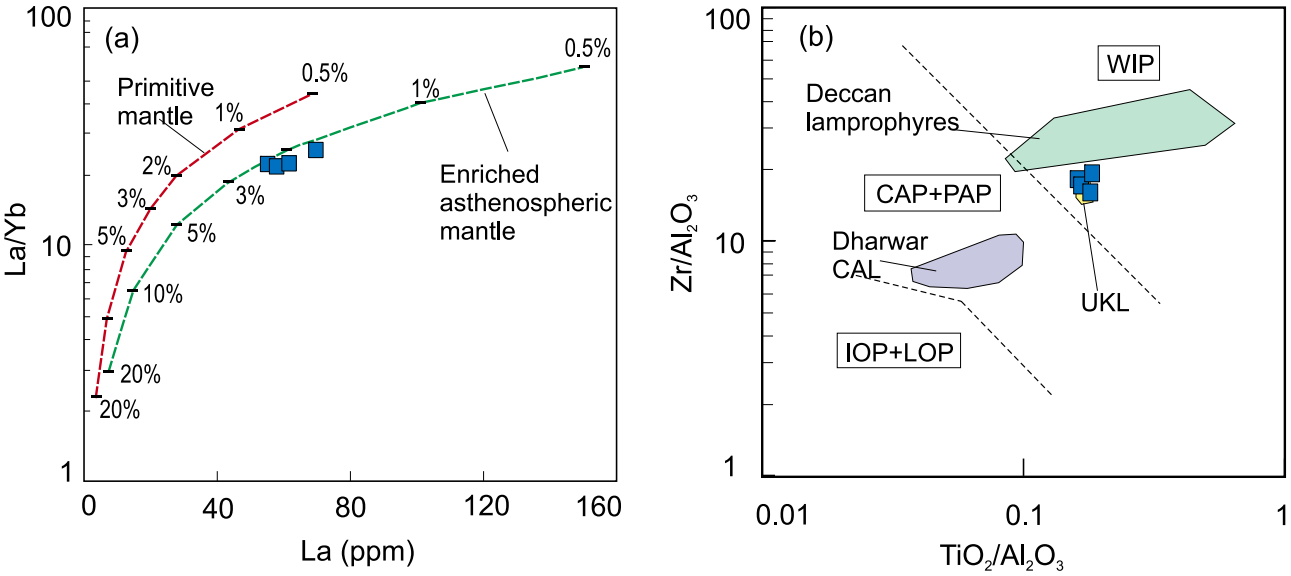

Figure 8. (a) La (ppm) versus La/Yb diagram showing melting curves for SPL samples. We have calculated the melting curves for garnet bearing PM (Primitive mantle) and EAM (enriched asthenospheric mantle) assuming a non-modal batch melting and taking initial modal mineralogy: Ol (55%) + Opx (19%) + Cpx (7%) + Gnt (11%) + Phl (8%) and melting phase proportions: Ol (5%) + Opx (12%) + Cpx (20%) + Gnt (40%) + Phl (23%) after from Miller et al. (1999). Various partition coefficients for olivine, pyroxene and garnet have been taken from Kostopoulos and James (1992) whereas those for phlogopite taken from Fujimaki et al. (1984). We have also calculated array for fractional crystallization (FC) assuming fractionation of olivine (40%) and clinopyroxene (60%) for every 10% increment. curves. We have taken source composition for PM after Sun and McDonough (1989) and for EAM after Seghedi et al. (2004). (b) Tectonic discrimination diagrams TiO_2/Al_2O_3 versus Zr/Al_2O_3 (after Muller and Groves, 2000), illustrating anorogenic within-plate geochemical character for ANL. Various fields and data sources are same as given in Figures 3 and 6. WIP, within plate; CAP, continental arc; PAP, post-collisional arc; IOP, initial arc; LOP, late oceanic arc.

reveals that the SPL generation can be explained by 1 to 3% of partial melting of EAM subsequently followed by fractionation of olivine and pyroxene and resembles that of the Udiripikonda lamprophyre.

Tectonomagmatic implication

Even though the SPL are temporally and spatially related to the Wajrakarur kimberlites, all of their respective Sr-Nd isotopes (Fig. 5) are contrasting. Whereas the Mesoproterozoic Wajrakarur field kimberlites were derived from an isotopically depleted mantle, the SPL tapped an enriched mantle source. In this aspect, SPL are similar to the nearby Udiripikonda shoshonitic lamprophyre. Pandey et al. (2017a, 2017b) advocated a subduction-linked subcontinental lithospheric mantle as a source for post-collisional calc-alkaline (Mudigubba and Kadiri) and shoshonitic lamprophyre (Udiripikonda) towards the western margin of Cuddapah basin (see Fig. 1 for locations). Our present study demonstrates that the studied Sivarampeta lamprophyres, despite being co-spatial to the above mentioned lamprophyre occurrences from EDC, show a mixed character and were derived from multiply modified heterogenous mantle source corresponding to Domain II (Giri et al. 2019) having a mixed sub-continental lithospheric mantle with an asthenospheric overprint. Such geochemical data would further help to characterize and model the heterogeneity of the mantle sources under the Indian continent through geological time.

CONCLUSIONS

Petrographic studies of the Sivarampeta lamprophyres suggest them to be calc-alkaline lamprophyres in general and kersantite in particular. Combined mineral chemistry and geochemistry reveals a mixed calc-alkaline and alkaline nature and highlight their shoshonitic character. Bulk rock geochemistry, and Sr-Nd isotope geochemistry suggest an enriched mantle source with the involvement of lithospheric-as well as asthenospheric components and belongs to the lamprophyres derived from the Domain II (Giri et al., 2019) in the eastern Dharwar craton. Petrogenetic modelling involving non- modal batch melting calculations reveal their melt generation from 1-3% melting of an enriched asthenospheric mantle that further underwent fractionation. Contrasting mantle sources were involved in the generation of Sivarampeta and co-eval and co-spatial kimberlites from the Wajrakarur kimberlite field implying mantle heterogeneity on a variable scale.

ACKNOWLEDGMENTS

We thank Kaushik Das for his invitation to contribute to this special issue. The Head, Department of Geology, BHU is thanked for his support. This research-work is an outcome of a major project (IR/S4/ESF-18/2011 dated 12.11.2013) sanctioned to NVCR by DST-SERB, New-Delhi. RKG & SR thanks UGC for awarding them JRF (NET). Suggestions by three anonymous journal reviewers and editorial comments by Kaushik Das are thankfully acknowledged.

SUPPLEMENTARY MATERIALS

Supplementary Table S1 and Figures S1-S4 are available online from https://doi.org/10.2465/jmps.191004b.

REFERENCES

Banerjee, A., Chakrabarti, R. and Mandal, S. (2016) Geochemical anatomy of a spheroidally weathered diabase. Chemical Geology, 117, 219-233.

Chalapathi Rao, N.V. (2008) Precambrian alkaline potassic-ultrapotassic, mafic-ultramafic magmatism in peninsular India. Journal of Geological Society of India, 72, 57-84.

Chalapathi Rao, N.V., Gibson, S.A., Pyle, D.M. and Dickin, A.P. (2004) Petrogenesis of Proterozoic lamproites and kimberlites from the Cuddapah basin and Dharwar craton, southern India. Journal of Petrology, 45, 907-948.

Chalapathi Rao, N.V., Dharma Rao, C.V. and Das, S. (2012) Petrogenesis of lamprophyres from Chhota Udepur area, Narmada rift zone, and its relation to Deccan magmatism. Journal of Asian Earth Sciences, 45, 24-39.

Chalapathi Rao, N.V., Wu, F.Y., Mitchell, R.H., Li, L.Q. and Lehmann, B. (2013) Mesoproterozoic U-Pb ages, trace element and Sr-Nd isotopic composition of perovskite from kimberlites of the Eastern Dharwar craton, southern India: Distinct mantle sources and a widespread 1.1 Ga tectonomagmatic event. Chemical Geology, 353, 48-64.

Chalapathi Rao, N.V., Dongre, A., Wu, F.-Y. and Lehmann, B. (2016) A Late Cretaceous (ca. 90 Ma) kimberlite event in southern India: Implication for sub continental lithospheric mantle evolution and diamond exploration. Gondwana Research, 35, 378-389.

Dawson, J.B. and Smith, J.V. (1977) The MARID (mica-amphibole-rutile-ilmenite-diopside) suite of xenoliths in kimberlite. Geochimica et Cosmochimica Acta, 41, 309-323.

Dongre, A., Chalapathi Rao, N.V., Viljoen, K.S. and Lehmann, B. (2017) Petrology, genesis and geodynamic implication of the Mesoproterozoic Late Cretaceous Timmasamudram kimberlite cluster, Wajrakarur field, eastern Dharwar craton, southern India. Geoscience Frontiers, 8, 541-553.

Fujimaki, H., Tatsumoto, M. and Aoki, K.-I. (1984) Partition coefficients of Hf, Zr and REE between phenocrysts and groundmasses. Journal of Geophysical Research, 89, 662-672.

Ganguly, J. and Bhattacharya, P.K. (1987) Xenoliths in Proterozoic kimberlites from southern India: petrology and geophysical implications, In Mantle Xenoliths (Nixon, P.H. Ed.). John Wiley, New York, 249-266.

Garza, A.O., Dostal, J., Keppie, J.D. and Paz-Moreno, F.A. (2013) Mid-Tertiary (25-21 Ma) lamprophyres in NW Mexico derived from subduction-modified subcontinental lithospheric mantle in an extensional backarc environment following steepening of the Benioff zone. Tectonophysics, 590, 59-71.

Gibson, S.A., Thompson, R.N., Leonardos, O.H., Dickin, A.P. and Mitchel, J.G. (1995) The Late Cretaceous impact of the Trindade mantle plume: evidence from largevolume, mafic, potassic magmatism in SE Brazil. Journal of Petrology, 36, 189-229.

Gibson, S.A., Thompson, R.N. and Day, J.A. (2006) Timescales and mechanisms of plume-lithosphere interactions: $^{40}Ar/^{39}Ar$ geochronology and geochemistry of alkaline igneous rocks from the Parana-Etendeka large igneous province. Earth and Planetary Science Letters, 251, 1-17.

Giri, R.K., Pankaj, P., Chalapathi Rao, N.V., Chakrabarti, R. and Pandit, D. (2019) Petrogenesis of an alkaline lamprophyre (camptonite) with ocean island basalt (OIB)-affinity at the NW margin of the Cuddapah basin, eatern Dharwar craton, southern India. Journal of Mineralogy and Geochemistry, 196/2, 149-177.

Ishwar-Kumar, Windley, B.F., Horie, K., Kato, T., et al. (2013) A Rodinia suture in western India: New insights on India-Madagascar correlations. Precambrian Research, 236, 227-251.

Jayananda, M., Peucat, J.-J., Chardon, D., Krishna Rao, B., et al. (2013) Neoarchean greenstone volcanism and continental growth, Dharwar Craton, southern India: constraints from SIMS U-Pb zircon geochronology and Nd isotopes. Precambrian Research, 227, 55-76.

Jayananda, M., Santosh, M. and Aadhiseshan, K.R. (2018) Formation of Archean (3600-2500 Ma) continental crust in the Dharwar Craton, southern India. Earth-Science Reviews, 181, 12-42.

Jiang, Y.-H., Jiang, S.-Y. and Ling, H.-F. (2010) Petrogenesis and tectonic implications of Late Jurassic shoshonitic lamprophyre dikes from the Liaodong Peninsula, NE China. Mineralogy and Petrology, 100, 127-151.

Karsli, O., Dokuz, A., Kaliwoda, M., Uysal, I., et al. (2014) Geochemical fingerprints of Late Triassic calc-alkaline lamprophyres from the Eastern Pontides, NE Turkey: A key to understanding lamprophyre formation in a subduction related environment. Lithos, 196, 181-197.

Khan, S., Dongre, A., Viljoen, F., Li, Q-L. and Roux, P.L. (2018) Petrogenesis of lamprophyres synchronous to kimberlites from the Wajrakarur kimberlite field: implications for contrasting lithospheric mantle sources and geodynamic evolution of the eastern Dharwar craton of southern India. Geological Journal, 1-23. DOI: 10.1002/gj.3394.

Kostopoulos, D.K. and James, S.D. (1992) Parametrization of the melting regime of the shallow upper mantle and the effects of variable lithosperic stretching on mantle modal stratification and trace element concentrations in magmas. Journal of Petrology, 33, 665- 691.

Krmicek, L., Cempírek, J., Havlín, A., Přichystal, A., et al. (2011) Mineralogy and petrogenesis of a Ba-Ti-Zr-rich peralkaline dyke from Šebkovice (Czech Republic): recognition of the most lamproitic Variscan intrusion. Lithos, 121, 74-86.

Krmicek, L., Romer, R.L., Ulrych, J., Glodny, J. and Prelevic, D. (2016) Petrogenesis of orogenic lamproites of the Bohemian Massif: Sr-Nd-Pb-Li isotope constraints for Variscan enrichment of ultra-depleted mantle domains. Gondwana Research,

35, 198-216.

La Flèche, M.R., Camiré, G. and Jenner, G.A. (1998). Geochemistry of post-Acadian, Carboniferous continental intraplate basalts from the Maritimes Basin, Magdalen Islands, Quebéc, Canada. Chemical Geology, 148, 115-136.

Le Maitre, R.W. (Ed.) (2002) Igneous Rocks: A Classification and Glossary of Terms. Recommendations of the International Union of Geological Sciences Subcommission on the Systematics of Igneous Rocks. pp. 236, Cambridge University Press, Cambridge.

Le Roex, A.P., Bell, D.R. and Davis, P. (2003) Petrogenesis of group I kimberlites from Kimberley, South Africa: evidence from bulk-rock geochemistry. Journal of Petrology, 44, 2261-2286.

Lefebvre, N., Kopylova, M. and Kivi, K. (2005) Archean calc-alkaline lamprophyres of Wawa, Ontario, Canada: Unconventional diamondiferous volcaniclastic rocks. Precambrian Research, 138, 57-87.

Leake, B.E., Woolley, A.R., Arps, C.E.S., Birch, W.D., et al. (1997) Nomenclature of amphiboles: report of the subcommittee on amphiboles of the international mineralogical association, commission on new minerals and mineral names. Canadian Mineralogist, 35, 219-246.

Li, X.Y., Zheng, J.P., Ma, Q., Xiong, Q., et al. (2014) From enriched to depleted mantle: Evidence from Cretaceous lamprophyres and Paleogene basaltic rocks in eastern and central Guangxi Province, western Cathaysia block of South China. Lithos, 184-187, 300-313.

Ma, L., Jiang, S.Y., Hou, M.L., Dai, B.Z., et al. (2014) Geochemistry of Early Cretaceous calc-alkaline lamprophyres in the Jiaodong Peninsula: Implication for lithospheric evolution of the eastern North China Craton. Gondwana Research, 25, 859-872.

Madhavan, V., David, K., Mallikharjuna Rao, J., Chalapathi Rao, N.V. and Srinivas, M. (1998) Comparative study of lamprophyres from the Cuddapah Intrusive Province (CIP) of Andhra Pradesh, India. Journal of Geological Society of India, 52, 621-642.

McKenzie, D. and O'Nions, R.K. (1991) Partial melt distributions from inversion of rare earth element concentrations. Journal of Petrology, 32, 1021-1091.

Miller, C., Schuster, R., Klötzli, U., Frank, W. and Purtscheller, F. (1999) Post-collisional potassic and ultrapotassic magmatism in SW Tibet: Geochemical and Sr-Nd-Pb-O isotopic constraints for mantle source characteristics and petrogenesis. Journal of Petrology, 40, 1399-1424.

Mitchell, R.H. (1995) Kimberlites, Orangeites and related Rocks. pp. 410, Plenum Press, New York.

Morimoto, N. (1988) Nomenclature of pyroxenes. Mineralogy and Petrology, 39, 55-76.

Moyen, J.-F., Martin, H., Jayananda, M. and Auvray, B. (2003) Late Archaean granites: a typology based on the Dharwar craton (India). Precambrian Research, 127, 102-123.

Muller, D. and Groves, D.I. (2000) Potassic Igneous Rocks and Associated Gold- copper Mineralization, 3rd ed. pp. 252, Springer, Berlin.

Muller, D. and Groves, D.I. (2019) Tectonic settings of Potassic Igneous rocks In Potassic Igneous Rocks and Associated Gold-Copper Mineralization. Mineral Resource Reviews, 31-71.

Naqvi S.M. (2005) Geology and Evolution of the Indian Plate (From Hadean to Holocene - 4 Ga to 4 Ka). pp. 450, Capital Publishing Company, New Delhi.

Nayak, S.S. and Kudari, S.A.D. (1999) Discovery of diamond bearing kimberlites in Kalyandurg area, Anantapur district, Andhra Pradesh. Current Science, 76, 1077-1079.

Orejana, D., Villaseca, C., Billström, K. and Paterson, B.A. (2008) Petrogenesis of Permian alkaline lamprophyres and diabases from the Spanish Central System and their geodynamic context within western Europe. Contributions to Mineralogy and Petrology, 156, 477-500.

Osborne, I., Sherlock, S., Anand, M. and Argles, T. (2011) New Ar-Ar ages of southern Indian kimberlites and a lamproite and their geochemical evolution. Precambrian Research, 189, 91-103.

Owen, J.P. (2008) Geochemistry of lamprophyres from the Western Alps, Italy: implications for the origin of an enriched isotopic component in the Italian mantle. Contributions to Mineralogy and Petrology, 155, 341-362.

Pandey, A., Chalapathi Rao, N.V., Pandit, D., Pankaj, P., et al. (2017a) Subduction tectonics in the evolution of the eastern Dharwar craton, southern India: Insights from the post-collisional calc-alkaline lamprophyres at the western margin of the Cuddapah basin. Precambrian Research, 298, 235-251.

Pandey, A., Chalapathi Rao, N.V., Chakrabarti, R., Pandit, D., et al. (2017b) Petrogenesis of a Mesoproterozoic shoshonitic lamprophyre dyke from the Wajrakarur kimberlite field, southern India: Geochemical and Sr-Nd isotopic evidence for a modified sub-continental lithospheric mantle source. Lithos, 292-293, 218-233.

Pandey, A., Chalapathi Rao, N.V., Chakrabarti, R., Pankaj, P., et al. (2018a) Post-collisional calc-alkaline lamprophyres from the Kadiri greenstone belt: evidence for the Neoarchean convergence-related evolution of the Eastern Dharwar Craton and its schist belts. Lithos, 320-321, 105-117.

Pandey, R., Chalapathi Rao, N.V., Dhote, P., Pandit, D., et al. (2018b) Rift-associated ultramafic lamprophyre (damtjernite) from the middle part of the Lower Cretaceous (125 Ma) succession of Kutch, northwestern India: Tectonomagmatic implications, Geoscience Frontiers, 9, 1883-1902.

Pandey, R., Pandey, A., Chalapathi Rao, N.V., Belyatsky, B., et al. (2019) Petrogenesis of end-Cretaceous/Early Eocene lamprophyres from the Deccan Large Igneous Province: Constraints on plume-lithosphere interaction and the post-Deccan lithosphere-asthenosphere boundary (LAB) beneath NW India. Lithos, 346-347.

Pearce, J.A. (2008) Geochemical fingerprinting of oceanic basalts with applications to ophiolite classification and the search for Archean oceanic crust. Lithos, 100, 14-48.

Peccerillo, A. and Taylor, S.R. (1976) Geochemistry of Eocene calc-alkaline volcanic rocks from the Kastamonu area, Northern Turkey. Contributions to Mineralogy and Petrology, 58, 63-81.

Pelletier, L., Vils, F., Kalt, A. and Gmeling, K. (2008) Li, B and Be contents of harzburgites from the Dramala complex (Pindos Ophiolite, Greece): Evidence for a MOR-type mantle in a supra-subduction zone environment. Journal of Petrology, 49, 2043-2080.

Peng, P., Qin, Z., Sun, F., Zhou, X., et al. (2019) Nature of charnockite and Closepet granite in the Dharwar Craton: Implications for the architecture of the Archean crust. Precambrian Research, 334, 1-15.

Peucat, J.-J., Jayananda, M., Chardon, D., Capdevila, R., et al. (2013) The lower crust of Dharwar craton, south India: Patch-

work of Archean granulitic domains. Precambrian Research, 227, 4–29.

Raghuvanshi, S., Pandey, A., Pankaj, P., Chalapathi Rao, N.V., et al. (2019) Lithosphere–asthenosphere interaction and carbonatite metasomatism in the genesis of Mesoproterozoic shoshonitic lamprophyres at Korakkodu, Wajrakarur kimberlite field, Eastern Dharwar Craton, southern India. In Special Issue: Evolution of the Indian subcontinent (Santosh, M., Ganguly, S., Rajesh,V.J., Hari, K.R. and Shaji, E. Eds.). Geological Journal, 54, 3060–3077.

Ramakrishnan, M. and Vaidyanadhan, R. (2008) Geology of India. pp. 556, Geological Survey of India (2 volumes).

Roberts, N.M.W. and Santosh, M. (2018) Capturing the Mesoarchean emergence of Continental crust in the Coorg Block, Southern India. American Geophysical Union, 45, 7444–7453.

Rock, N.M.S. (1986) The nature and origin of ultramafic lamprophyres: Alnöites and allied rocks. Journal of Petrology, 27, 155–196.

Rock, N.M.S. (1987) The nature and origin of lamprophyres: an overview. In Alkaline Igneous Rocks (Fitton, J.G. and Upton, B.G.J. Eds.). Geological Society of London Special Publications, 191–226.

Rock, N.M.S. (1991) Lamprophyres. pp. 225, Blackie, London.

Rudnick, R.L., Mcdonough, W.F. and Orpin, A. (1994) Northern Tanzanian peridotite xenoliths: a comparison with Kaapvaal peridotites and inferences on metasomatic interactions. In Kimberlites, Related Rocks and Xenoliths. Proceedings of the 5th International Kimberlite Conference (Meyer, H.O.A. and Leorandos, O.H. Eds.). CPRM (Companhia de Pesquisa de Recursos Minerais), Special Publications, 336–354.

Rudnick, R.L. and Gao, S. (2003) Composition of the continental crust. In The Crust (Holland, H.D. and Turekian, K.K. Eds.). Treatise on Geochemistry, 3, 1–64.

Santosh, M., Yang, Q.–Y., Tsunogae, T., Ram Mohan, M. and Satyanarayan, M. (2015) An exotic Mesoarchean microcontinent: The Coorg Block, southern India. Gondwana Research, 27, 165–169.

Seghedi, I., Downes, H., Vaselli, O., Szaka'cs, A., et al. (2004) Postcollisional Tertiary–Quaternary mafic alkalic magmatism in the Carpathian–Pannonian region: a review. Tectonophysics, 393, 43–62.

Stoppa, F., Rukhlov, A.S., Bell, K., Schiazza, M. and Vichi, G. (2014) Lamprophyres of Italy: early Cretaceous alkaline lamprophyres of Southern Tuscany, Italy. Lithos, 188, 97–112.

Su, H.M., Jiang, S.Y., Zhang, D.Y. and Wu, X.K. (2017) Partial melting of subducted sediments produced early Mesozoic calc–alkaline lamprophyres from northern Guanxi Province, South China. Scientific Reports, 7, 4864.

Sun, C.M. and Bertrad, J. (1991) Geochemistry of clinopyroxenes in plutonic and volcanic sequences from the Yanbian Proterozoic ophiolites (Sichuan Province, China): petrogenetic and geotectonic implications. Schweizer Minealogische und Petrographische Mitteilungen, 71, 243–259.

Sun, S.S. and McDonough, W.F. (1989) Chemical and isotopic systematics of oceanic basalts: implications for mantle composition and processes. In Magmatism in Ocean Basins (Saunders, A.D. and Norry, M.J. Eds.). Geological Society of London, Special Publlication, 42, 313–345.

Swami Nath, J., Ramakrishnan, M. and Viswanatha, M.N. (1976) Dharwar stratigraphic model and Karnataka craton evolution. Records of Geological Survey of India, 107, 149–175.

Takahashi, E., Uto, K. and Schilling, J.–G. (1987) Primary magma compositions and Mg/Fe ratios of their mantle residues along Mid Atlantic Ridge 29°N to 73°N. Technical Report of ISEI, Okayama University 9, 1–4.

Taylor, W.R., Rock, N.M. and Groves, D.I. (1994) Geochemistry of Archean shoshonitic lamprophyres from the Yilgarn Block, Western Australia: Au abundance and association with gold mineralization. Applied Geochemistry, 9, 197–222.

Woolley, A.L., Bergman, S.C., Edgar, A.D., Le Bas, M.J., et al. (1996) Classification of lamprophyres, lamproites, kimberlites, and the kalsilitic, melilitic, and leucitic rocks. Candian Mineralogist, 34, 175–186.

Wyman, D.A. and Kerrich, R. (1989) Archean lamprophyres of the Superior Province, Canada: distribution, petrology, and geochemical characteristics. Journal of Geophysical Research, 94B, 4667–96.

Wyman, D.A. and Kerrich, R. (1993) Archean shoshonitic lamprophyres of the Abitibi Subprovince, Canada: Petrogenesis, Age and tectonic setting. Journal of Petrology, 34, 1067–1109.

Manuscript received October 4, 2019
Manuscript accepted March 13, 2020
Published online March 31, 2020
Manuscript handled by Kaushik Das Guest Editor